

The nature of EU Pegasi: An Algol-type binary with a δ Scuti-type component

Yuanguai YANG,^{1,*} Huiyu YUAN,^{1,*†} Haifeng DAI,¹ and Xiliang ZHANG²

¹Information College/School of Physics and Electronic Information, Huaibei Normal University, Huaibei 235000, Anhui Province, China

²Yunnan Observatories, Chinese Academy of Sciences, 396 Yangfangwang, Guandu District, Kunming 650216, China

*E-mail: yuanhy@chnu.edu.cn (HY); yygc@163.com (YY)

Received 2017 June 23; Accepted 2017 December 22

Abstract

The comprehensive photometry and spectroscopy for the neglected eclipsing binary EU Pegasi are presented. We determine its spectral type to be A3V. With the W-D program, the photometric solution was deduced from the four-color light curves. The results imply that EU Peg is a detached binary with a mass ratio of $q = 0.3105(\pm 0.0011)$, whose components nearly fill their Roche lobes. The low-amplitude pulsation occurs around the secondary eclipse, which may be attributed to the more massive component. Three frequencies are preliminarily explored by the Fourier analysis. The pulsating frequency at $f_1 = 34.1 \text{ cd}^{-1}$ is a p -mode pulsation. The orbital period may be undergoing a secular decrease, superimposed by a cyclic variation. The period decreases at a rate of $dP/dt = -7.34 \pm 1.06 \text{ d yr}^{-1}$, which may be attributed to mass loss from the system due to stellar wind. The cyclic oscillation, with $P_{\text{mod}} = 31.0 \pm 1.4 \text{ yr}$ and $A = 0.0054 \pm 0.0010 \text{ d}$, may be caused by the light-time effect due to the assumed third body. With its evolution, the pulsating binary EU Peg will evolve from the detached configuration to the semi-detached case.

Key words: binaries: eclipsing — stars: individuals (EU Pegasi) — stars: variables: delta Scuti

1 Introduction

Pulsations in eclipsing binaries are of particular interest for the theories of stellar formation, structure, and evolution because binarity may provide accurate physical parameters of both components. It may tell us about the internal structure of the pulsating star, especially for our Sun (Gough 2000). Therefore, it is important for us to probe such pulsations in helioseismology of eclipsing binaries (Aerts 2007; Huber 2015), to help us to identify pulsating modes and compare the results from stellar theory. The pulsations of eclipsing binaries have not been adequately investigated since the δ Scuti-type pulsations in AB Cas were first discovered by Tempesti (1971). In detached and

semi-detached binaries, mass transfer, accretion, and gas envelopes may influence pulsation (Mkrtrichian et al. 2005). Although dozens of sample binaries have been observed (Liakos et al. 2012; Zhang et al. 2013; Yang et al. 2014), the problem of mode identification and shortcomings in the stellar models are major difficulties (Pamyatnykh et al. 1998). The pulsation modes have been detected and their frequencies determined by many authors. Zhang, Luo, and Fu (2013) and Cakirli and İbanoğlu (2016) derived the correction between orbital and dominant pulsation periods. The threshold orbital period of $\sim 13 \text{ d}$ may be an apparent limit, beyond which the intrinsic pulsations for the δ Scuti stars may not be affected by the binarity (Liakos &

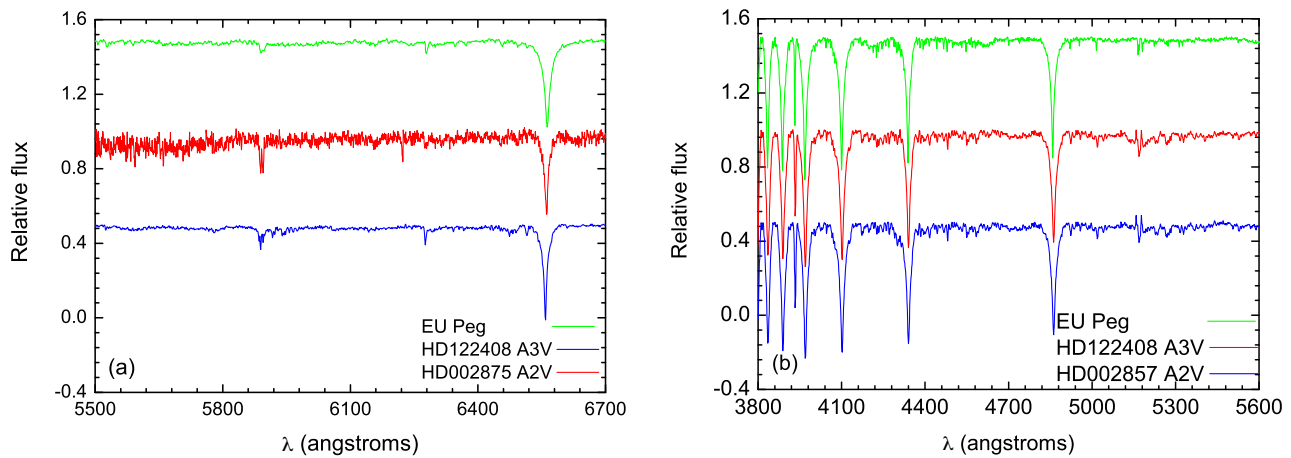


Fig. 1. Normalized spectra of the eclipsing binary EU Peg, observed on 2016 October 8 (a) and October 23 (b). The spectrum data are added with displacements of +0.5 for HD 002857 and -0.5 for HD 122408. (Color online)

Niarchos 2015). Liakos and Niarchos (2017) published a catalogue with properties of 118 δ Scuti stars in binaries. There were only two pulsating binaries with less than 0.7 d periods: VV UMa ($P = 0.6874$ d; Kim et al. 2005) and V1464 Aql ($P = 0.6978$ d; Dal & Sipahi 2013). Therefore, searching for short-period eclipsing binaries with pulsations is helpful for us to understand their pulsating mechanisms.

EU Peg (= 2MASS J23012519+2720211) is an Algol-type eclipsing binary with EA-type light curves (Budding et al. 2004). Malkov et al. (2006) classified it to be in “semi-detached status” and assigned its spectral type to be (A8) + [G2IV]. The visual magnitude ranges from 12.20 mag to 12.80 mag (Kukarkin et al. 1971). The orbital period of EU Peg was reported as 0.7211 d, and refined to be 0.721113 d (Keriner 2004). No determinations for this binary have been made of the physical properties, and the system has since been generally neglected except for measurements of the times of eclipse.

In this paper, we found a δ Scuti component in the EU Peg binary system, which is the third short-period pulsating binary. In section 2, the photometry and spectroscopy for this binary are first presented. On the basis of two spectrograms, we determined the spectral type. Section 3 is devoted to studying possible period variations. Models for the four-band light curves and pulsation analysis are given in section 4, in which we obtain the photometric elements and pulsating frequencies. Finally, we discuss the evolutionary state and causes of period changes.

2 Data and data reduction

2.1 Spectroscopy

Two low-resolution spectrograms for EU Peg were observed by using the OMR spectrograph of the 2.16 m telescope

at the Xinglong station (XLs) of National Astronomical Observatories of China (NAOC) on 2016 October 8, and the Beijing Faint Object Spectrograph and Camera (BFOSC) of the 2.4 m telescope at the Lijiang station of Yunnan Astronomical Observatory (YNAO) on 2016 October 23, respectively. For the 2.16 m telescope, we chose a slit width of $1''.8$ and the Grism-14 with a wavelength ranging from 3200 \AA to 7500 \AA (Fan et al. 2015). Its exposure time is 10 min. For the 2.4 m telescope, meanwhile, we used the grating of $1200 \text{ lines mm}^{-1}$, which results in a wavelength coverage of $\sim 1380 \text{ \AA}$ (Fan et al. 2016). The exposure time is 15 min. Reduction of the spectra was performed by using IRAF packages,¹ including bias subtraction, flat-fielding, and cosmic-ray removal. Finally, the one-dimensional spectrum was extracted. Using the *winnmk* software,² two normalized spectra are displayed in figure 1. The spectra of two standard stars, HD 122408 and HD 002857,³ are also plotted in both panels. The spectrum of figure 1 a is extremely noisy, although the double lines for Na and the $H\alpha$ line are evident. Due to the lack of short wavelength, we re-observed this binary using the 2.4 m telescope and obtained the spectrum shown in figure 1b. On the basis of the stellar spectral classification (Gray & Corbally 2009), we determined its spectral type to be A3V, which differs from the estimated spectral type of (A8) + [G2IV] (Malkov et al. 2006).

2.2 CCD photometry

Comprehensive photometry for EU Peg was carried out from 2013 September 25 to November 11 with the 85 cm

¹ IRAF is supported by the National Optical Astronomy Observatories (NOAO) in Tucson, Arizona (<http://iraf.noao.edu/iraf/web/iraf-homepage.html>).

² (<http://www.appstate.edu/~grayro/MK/winnmk.htm>).

³ (<http://www.ast.obs-mip.fr/users/leborgne/stelib/stars.html>).

Table 1. Multicolor photometric observations for EU Peg.*

60 cm telescope				85 cm telescope					
B band		V band		V band		R _c band		I _c band	
JD (Hel.)	Δm	JD (Hel.)	Δm	JD (Hel.)	Δm	JD (Hel.)	Δm	JD (Hel.)	Δm
601.98744	+0.053	576.15711	+0.126	560.96598	+0.111	560.96656	+0.214	561.05232	+0.330
601.98868	+0.051	576.15750	+0.126	560.96715	+0.117	560.96773	+0.218	561.05362	+0.324
601.98992	+0.044	576.15790	+0.125	560.96831	+0.118	560.96890	+0.219	561.05558	+0.327
601.99116	+0.050	576.15829	+0.121	560.96948	+0.124	560.97006	+0.224	561.05689	+0.348
601.99258	+0.046	576.15869	+0.133	560.97065	+0.122	560.97123	+0.221	561.05819	+0.339
601.99405	+0.048	576.15908	+0.130	560.97181	+0.117	560.97238	+0.216	561.05949	+0.343
601.99552	+0.056	576.15948	+0.127	560.97297	+0.115	560.97355	+0.214	561.06079	+0.352
601.99699	+0.048	576.15987	+0.138	560.97413	+0.117	560.97472	+0.220	561.06209	+0.342
601.99847	+0.043	576.16026	+0.129	560.97530	+0.110	560.97588	+0.213	561.06339	+0.341
601.99997	+0.048	576.16066	+0.124	560.97647	+0.118	560.97705	+0.222	561.06468	+0.354
602.00148	+0.036	576.16105	+0.127	560.97763	+0.119	560.97822	+0.217	561.06599	+0.338
602.00300	+0.044	576.16145	+0.124	560.97880	+0.119	560.97938	+0.221	561.06729	+0.352

*All the individual data are available in the online edition as supplementary data.

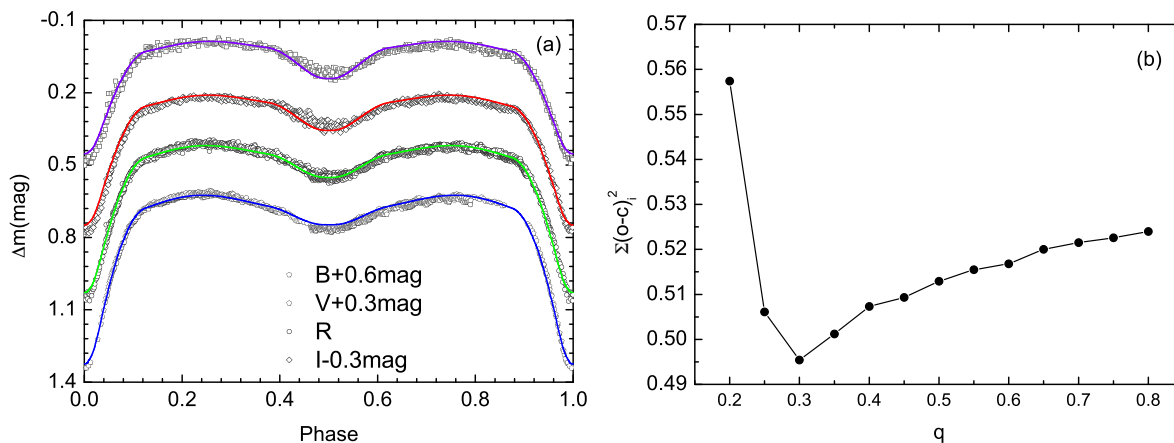


Fig. 2. BVR_cI_c -band light curves of EU Peg (a). The solid color lines show the photometric solution (see table 5). The resulting $\Sigma(q)$ curve (b) is deduced from all the photometric data. (Color online)

telescope (Zhou et al. 2009) and the 60 cm telescope (Yang et al. 2010) at XLs of NAOC. The standard Johnson–Cousin–Bessel $UBVR_cI_c$ systems are mounted on two small telescopes. The photometric effective images were reduced by using the IMRED and APPHOT packages in IRAF, after we performed bias and dark subtraction, and flat-field correction. We then obtained the differential magnitudes between the variable and the comparison star.

In the observing process, TYC 2243-709-1 ($B = 11.88$, $V = 11.22$) and TYC 2243-1242-1 ($B = 11.98$, $V = 11.09$) were chosen to be the comparison and check stars, respectively. Typical exposure times were generally set to be 50 s for B , 40 s for V , 30 s for R_c , and 25 s for the I_c band, which depends on the weather condition. Most useful observations were obtained over nine nights. In total, we obtained

4565 effective CCD images. Table 1 lists the heliocentric Julian dates (HJDs) and the differential magnitudes with respect to the comparison star. The *comparison – check* magnitude differences, i.e., rms scatters, are 0.007 mag in B and 0.006 mag in the V band for the 60 cm telescope, and 0.013 mag in V , 0.014 mag in R_c , and 0.022 in the I_c band for the 85 cm telescope, respectively. The complete light curves are shown in figure 2a, in which the phases are computed by the new linear ephemeris in equation (1) in section 3. From this figure, the brightness fluctuations, especially in the B and V bands, occur during the secondary minima and disappear near the central phase of the primary minima, which is similar to another previously studied star FR Ori (Yang et al. 2014). The low-amplitude pulsations in the BV light curves are displayed in figure 3, which were obtained only on the fine nights. The pulsations occurring

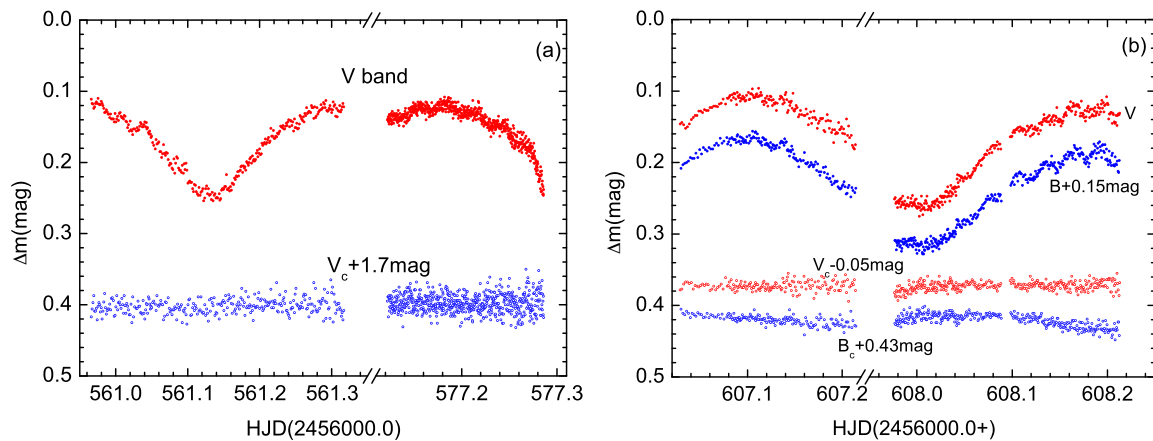


Fig. 3. Pulsating light variations with low amplitudes around secondary minima for EU Peg, observed using the 85 cm telescope (a) and the 60 cm telescope (b) at XLs of NAOC in 2013. In the lower part of both panels, the “Bc” and “Vc” values are in the sense of *comparison – check* with magnitude displacements. (Color online)

Table 2. New observed eclipsing times for EU Peg.

JD (Hel.)	Error	Filter	Min.	Telescope
2456561.13335	± 0.00065	V	II	85 cm
2456561.13790	± 0.00100	R _c	II	85 cm
2456561.13238	± 0.00066	I _c	II	85 cm
2456562.21142	± 0.00023	V	I	85 cm
2456562.20989	± 0.00019	R _c	I	85 cm
2456562.21184	± 0.00023	I _c	I	85 cm
2456604.03722	± 0.00019	B	I	60 cm
2456606.20108	± 0.00057	B	I	60 cm
2456606.20121	± 0.00069	V	I	60 cm

at the secondary eclipses imply that the more massive component in the EU Peg binary may be a δ Scuti-type star.

3 Orbital period variations

From our new data, we determined four light minimum times, listed in table 2. From the $O - C$ gateway,⁴ a total of 34 eclipse times (i.e., 11 photographic, 3 photoelectric, and 20 CCD) was compiled to study the period changes. Table 3 gives those data with their errors and measurement methods. For all the eclipsing times, individual weights are assigned inversely proportional to their standard errors. However, the uncertainties for some timings could not be given. Therefore, we have assumed errors of ± 0.001 d for the 11 photographic data, and ± 0.0005 d for two of the photoelectric ones (Hübscher et al. 1994), respectively. Based on all the times of minimum light, a weighted least-squares method yields a new linear ephemeris as follows:

$$\text{Min. I} = \text{HJD } 2456562.2086(11) + 0.72111515(8) \times E, \quad (1)$$

⁴ (<http://var2.astro.cz/ocgate/>).

in which the numbers in parentheses show the errors in the last decimal place. The initial timing residuals with respect to equation (1), $(O - C)_i$, are listed in table 3 and displayed in figure 4a. From this figure, the orbital period of EU Peg clearly displays a secular decrease with some irregular oscillations, although a 36-year gap exists between HJD 2435401.078 (Kaho 1952) and HJD 2448465.538 (Hübscher et al. 1995). Therefore we have assumed that the $(O - C)_i$ curve may be described by a downward parabola with a sinusoidal curve, similar to the case occurring in the binary SX Dra (Soydugan & Kaçar 2013). By using a nonlinear least-squares method with weights, the following equation was used to represent the cyclic variation and parabola of the $(O - C)$ data:

$$\text{Min. I} = T_0 + P \times E + Q \times E^2 + A_{\text{mod}} \times \sin \left[\frac{2\pi}{P_{\text{mod}}} (E - T_s) \right], \quad (2)$$

where A_{mod} , P_{mod} , and T_s are the amplitude, period, and moment of the minimum of the sinusoidal variation, while T_0 , P , Q , and E are the epoch, the orbital period of the binary system, the coefficient of the quadratic term, and the epoch number, respectively. The fitting parameters are listed in table 4. From equation (2), we obtained the computed values, $(O - C)_{\text{parab}}$ and $(O - C)_c$, for all eclipsing times, which are listed in table 3. From the coefficient of the quadratic term, Q , we determined a period decrease rate of $dP/dt = -7.34(\pm 1.06) \times 10^{-7} \text{ d yr}^{-1}$. As shown in figure 4a, the solid and dotted lines are plotted from equation (2) and only its parabolic part, respectively.

After being removed from $(O - C)_i$ by the best parabolic fit of equation (2), the $(O - C)_c$ residuals are displayed in figure 4b. The cyclic change is plotted as a solid line

Table 3. All available times of light minima for EU Peg.

JD (Hel.)	Error	Epoch	Method	(O - C) _i (d)	(O - C) _{parab} (d)	(O - C) _c (d)	(O - C) _f (d)	Reference
2433981.919*	±0.001	-31313.0	pg	-0.0109	-0.0136	+0.0053	-0.0026	Kaho (1952)
2434302.106*	±0.001	-30869.0	pg	+0.0009	-0.0125	+0.0054	+0.0080	Kaho (1952)
2434628.044*	±0.001	-30417.0	pg	-0.0051	-0.0114	+0.0054	+0.0009	Kaho (1952)
2435044.125*	±0.001	-29840.0	pg	-0.0076	-0.0100	+0.0051	-0.0026	Kaho (1952)
2435401.078*	±0.001	-29345.0	pg	-0.0066	-0.0089	+0.0046	-0.0022	Kaho (1952)
2448465.538*	±0.001	-11228.0	pg	+0.0103	+0.0083	+0.0003	+0.0017	Hübscher, Agerer, and Wunder (1995)
2448499.421*	±0.001	-11181.0	pg	+0.0009	+0.0083	+0.0002	-0.0076	Hübscher, Agerer, and Wunder (1992)
2448501.588*	±0.001	-11178.0	pg	+0.0045	+0.0083	+0.0002	-0.0039	Hübscher, Agerer, and Wunder (1992)
2448514.566*	±0.001	-11160.0	pg	+0.0024	+0.0083	+0.0001	-0.0060	Hübscher, Agerer, and Wunder (1992)
2448840.509*	±0.001	-10708.0	pg	+0.0014	+0.0081	-0.0008	-0.0058	Hübscher and Agerer (1996)
2448988.344*	±0.001	-10503.0	pg	+0.0078	+0.0080	-0.0013	+0.0011	Hübscher and Agerer (1993)
2449202.5194†	±0.0005	-10206.0	pe	+0.0120	+0.0078	-0.0019	+0.0060	Hübscher et al. (1994)
2449249.3863†	±0.0005	-10141.0	pe	+0.0064	+0.0078	-0.0020	+0.0006	Hübscher et al. (1994)
2450671.4216	±0.0011	-8169.0	CCD	+0.0026	+0.0065	-0.0050	+0.0011	Agerer, Dahm, and Hübscher (1999)
2451796.3545	±0.0006	-6609.0	CCD	-0.0041	+0.0051	-0.0053	-0.0039	Diethelm (2000)
2452147.5456	±0.0024	-6122.0	CCD	+0.0039	+0.0045	-0.0049	+0.0043	Zejda (2004)
2452150.4268	±0.0002	-6118.0	CCD	+0.0007	+0.0045	-0.0049	+0.0011	Agerer and Hübscher (2003)
2452535.5020	±0.0005	-5584.0	CCD	+0.0004	+0.0039	-0.0044	+0.0008	Diethelm (2013)
2452581.6528	±0.0002	-5520.0	CCD	-0.0002	+0.0038	-0.0043	+0.0002	Dvorak (2003)
2452913.3646	±0.0002	-5060.0	CCD	-0.0014	+0.0033	-0.0036	-0.0011	Hübscher (2005)
2454421.9390	±0.0005	-2968.0	CCD	+0.0001	+0.0003	+0.0006	-0.0008	Nagai (2008)
2455500.7279	±0.0004	-1472.0	CCD	+0.0008	-0.0022	+0.0035	-0.0006	Diethelm (2012)
2455854.7967	±0.0001	-981.0	CCD	+0.0020	-0.0031	+0.0042	+0.0008	J. M. Kreiner (2011 private communication)
2455862.7278	±0.0001	-970.0	CCD	+0.0009	-0.0031	+0.0043	-0.0003	J. M. Kreiner (2011 private communication)
2455863.8085	±0.0003	-968.5	CCD	-0.0001	-0.0031	+0.0043	-0.0013	J. M. Kreiner (2011 private communication)
2455875.7051	±0.0003	-952.0	CCD	-0.0019	-0.0031	+0.0043	-0.0031	Diethelm (2011)
2456132.4214	±0.0002	-596.0	pe	-0.0026	-0.0038	+0.0047	-0.0035	Hübscher (2014)
2456232.6571	±0.0003	-457.0	CCD	-0.0019	-0.0040	+0.0049	-0.0027	Diethelm (2003)
2456561.1345	±0.0008	-1.5	CCD	+0.0076	-0.0049	+0.0052	+0.0073	Present paper
2456562.2111	±0.0002	+0.0	CCD	+0.0024	-0.0049	+0.0052	+0.0022	Present paper
2456604.0372	±0.0002	+58.0	CCD	+0.0039	-0.0051	+0.0052	+0.0037	Present paper
2456606.2012	±0.0006	+61.0	CCD	+0.0045	-0.0051	+0.0052	+0.0043	Present paper
2457267.4572	±0.0002	+978.0	CCD	-0.0021	-0.0070	+0.0054	-0.0005	Juryšek et al. (2017)
2457324.4250	±0.0001	+1057.0	CCD	-0.0023	-0.0071	+0.0054	-0.0006	Juryšek et al. (2017)

*For the 11 photographic data, we assumed their observed errors to be ±0.001 d.
 †For two of the photoelectric data (Hübscher et al. 1995), their uncertainties are taken as ±0.0005 d.

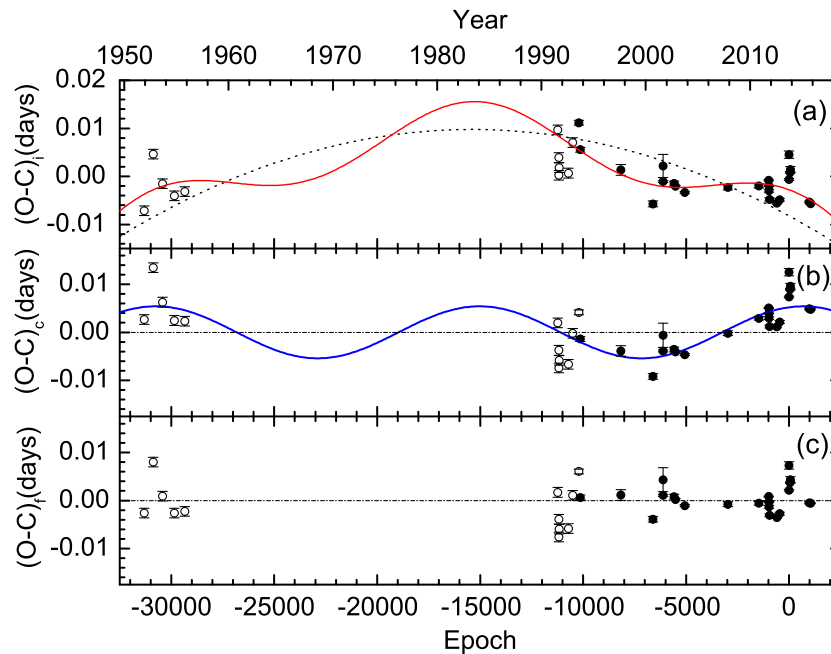


Fig. 4. Residual diagrams: $(O - C)_i$ (a), $(O - C)_c$ (b), and $(O - C)_f$ (c). The open and filled circles represent the photographic and the photoelectric/CCD measurements, respectively. In panel (a), the solid and dotted lines are computed from equation (2) and only its parabolic part, respectively. Meanwhile, the continuous curve in panel (b) is plotted by the sinusoidal term of equation (2). (Color online)

Table 4. New ephemeris of EU Peg.

Quadratic plus sinusoidal fitting

$$\text{Min.I (HJD)} = T_0 + E \times P + Q \times E^2 + A \times \sin \left[\frac{2\pi}{P_{\text{mod}}} (E - T_s) \right]$$

$$T_0 = \text{HJD } 2456562.2037(\pm 0.0008)$$

$$P = 0.72111515(\pm 0.00000028) \text{ d}$$

$$Q = -7.24(\pm 1.05) \times 10^{-11} \text{ d}$$

$$A_{\text{mod}} = 0.0054(\pm 0.0010) \text{ d}$$

$$P_{\text{mod}} = 11327(\pm 570) \text{ d} = 31.0(\pm 1.4) \text{ yr}$$

$$T_s = 12470(\pm 400) \text{ epochs}$$

from the sinusoidal term of equation (2). The period of this oscillation is $P_{\text{mod}} = 31.0(\pm 1.4)$ yr. From the fit including both quadratic and sinusoidal terms, we obtained the final residuals $(O - C)_f$, which are listed in table 3 and shown in figure 4c. From this figure, no regularity is found. Therefore, equation (2) is acceptable for us to fit all the data, although a large gap exists. In future observations, more eclipsing times are needed to check the behavior of the orbital period variations.

4 Analyzing light curves

From the light curves of figure 2a, EU Peg is identified to be an Algol-type eclipsing binary. The photometric elements are deduced from four-color light curves, including 912 data in the B band, 2729 in the V band, 806 in the R_c band, and 741 in the I_c band. After the binary solution

was removed from the observations (i.e., the light-curve residuals), a Fourier analysis was performed on the residuals in order to study the pulsation behavior of the primary component.

4.1 Photometric solution

Theoretical light curves of EU Peg were simultaneously computed by the 2015 version of the W-D program⁵ (Wilson & Devinney 1971; Wilson & Van Hamme 2014). The limb-darkening coefficients were generated with the LC and DC programs. In the calculating process, we fixed $LD_1 = LD_2 = -2$ for the bolometric logarithmic limb-darkening law (van Hamme & Wilson 2007), and $MREF = 2$ for the detailed reflect model (Wilson 1979). Assuming the spectral type of A3V with an uncertainty of a subtype for EU Peg, the mean effective temperature for Star 1 may be estimated to be $T_1 = 8730(\pm 270)$ K, based on the calibration of MK spectral types (Cox 2000). The gravity-darkening exponents and bolometric albedo coefficients were fixed to be $g_1 = 1.0$ (von Zeipel 1924), $g_2 = 0.32$ (Lucy 1967), $A_1 = 1.0$, and $A_2 = 0.5$ (Rucinski 1973), respectively. As usual, the other adjustable parameters are T_0 , P_0 , T_2 , i , q , Ω_1 , Ω_2 , and ℓ_3 in solving the light curves.

In order to determine a mass ratio, we performed a q -search process on all the data. The solutions tried imply

⁵ FTP site (<ftp://ftp.astro.ufl.edu/pub/wilson/lcdc2015>).

Table 5. Geometrical and physical parameters for EU Peg.

Parameter	Primary	Secondary
T (K)	$8730 \pm 270^*$	5064 ± 12
T_0 (HJD)	$2456562.2117(\pm 0.0002)$	
P_0 (d)	$0.72113316(\pm 0.00000192)$	
i ($^\circ$)	81.3 ± 0.8	
$q = M_2/M_1$	0.3105 ± 0.0011	
$\Omega_{1,2}$	2.8713 ± 0.0031	2.5938 ± 0.0041
$L_i/(L_1 + L_2)_B$	0.9829 ± 0.0055	0.0171
$L_i/(L_1 + L_2)_V$	0.9650 ± 0.0057	0.0350
$L_i/(L_1 + L_2)_{R_c}$	0.9474 ± 0.0065	0.0526
$L_i/(L_1 + L_2)_{I_c}$	0.9269 ± 0.0087	0.0731
ℓ_{3B} (%)	0.25 ± 0.04	
ℓ_{3V} (%)	0.39 ± 0.04	
ℓ_{3R_c} (%)	0.68 ± 0.05	
ℓ_{3I_c} (%)	1.02 ± 0.07	
r (pole)	0.3954 ± 0.0022	0.2429 ± 0.0018
r (point)	0.4398 ± 0.0035	0.2875 ± 0.0087
r (side)	0.4134 ± 0.0034	0.2506 ± 0.0020
r (back)	0.4256 ± 0.0025	0.2714 ± 0.0023
$\langle r \rangle^\dagger$	0.4185 ± 0.0032	0.2631 ± 0.0037
a (R_\odot)	5.09 ± 0.20	
M (M_\odot)	$2.60 \pm 0.30^\ddagger$	0.81 ± 0.10
R (R_\odot)	2.13 ± 0.02	1.34 ± 0.02
L (L_\odot)	23.65 ± 0.36	1.06 ± 0.03

*The mean effective temperature for the more massive component is fixed from the spectral type of A3V with an uncertainty of a subtype.

† Bracket indicates the equal-volume radius.

‡ Based on A3V with a subtype error, the mass for the primary component (i.e., star 1) was estimated (Cox 2000).

that EU Peg has a detached configuration, rather than a semi-detached one (Budding et al. 2004). The relation between q and Σ is shown in figure 2b, in which a minimum value of Σ appears at around a mass ratio of 0.3. The mass ratio q and third light ℓ_3 are then considered to be free parameters. The final photometric elements are listed in table 5. The fill-out factor is computed by $f = \langle r \rangle / r_{\text{cr}}$, in which r_{cr} is the equivalent relative radius of the Roche lobe (Eggleton 1983). The values for both components are $f_p = 86.7(\pm 0.6)\%$ and $f_s = 92.6(\pm 0.1)\%$. The computed light curves are plotted as solid lines in figure 2a. From this figure, the R_c and I_c light curves may be not fitted well, which may be due to the different filters. The contributions to the total light, ℓ_3 , are 0.25%, 0.39%, and 0.68%, and 1.02% in the B , V , R_c , and I_c bands, respectively.

4.2 Pulsating frequency analysis

To explore the pulsating frequencies, small-amplitude pulsations were analyzed after being removed by the binary solution from the light curves. From figure 3, the pulsations occur around both light maxima, and may result from the more massive component, possibly in the instability strip of

the H–R diagram. This kind of pulsation occurs in another short-period ($P < 1$ d) detached Algol-type binary, HZ Dra (Liakos et al. 2012). After the eclipses and proximity effects of the binary were removed by theoretical light curves, we obtained 5.9 hr in the V band (from the 85 cm telescope), and 4.2 hr in the B and V bands (from the 60 cm telescope) residual data. Due to only 10.1 hr pulsations (i.e., 225 in the B band and 917 in the V band), searching for pulsation frequencies is then preliminary. As shown in figure 5, a total of 1142 residual observations were analyzed using the Period04 software⁶ (Lenz 2004; Lenz & Breger 2005), which is based on the classical discrete Fourier transform and multiple-least-squares algorithms.

When we calculated the frequencies, the residual light curves were subsequently pre-whitened one by one. The signal/noise amplitude ratio is $S/N \sim 4.0$ as a good criterion to distinguish between peaks due to pulsation and noise (Breger et al. 1993). The analyses were performed for the B data, the V data, and all the data together, respectively. The detected frequencies are listed in table 6, in which the uncertainties of the parameters are computed by the formulae from Montgomery and O’Donoghue (1999). The observed noises are $\sigma(m)_B = 0.0071$ mag, $\sigma(m)_V = 0.0113$ mag, and $\sigma(m)_{B+V} = 0.0106$ mag, respectively. From table 5, three frequencies from the V data approximately agree with those from all the data. For 225 data points in the B band, the only reliable result may be the frequency of f_1 . So we accept the results derived from the data in the B and V bands. The spectral window and amplitude spectra are displayed in figure 6, although three peaks are not prominent due to pulsating observations with a short duration of 10.1 hr. Using the estimated parameters in table 4, the mean density of the primary can be computed to be $\rho_1/\rho_\odot = (M_1/M_\odot)/(R_1/R_\odot)^3 = 0.2685(\pm 0.0370)$. Following the formula of $Q = P_{\text{pul}}(\rho/\rho_\odot)$, we can calculate the pulsating constant for each frequency. The theoretical curves are plotted in figure 5 as solid lines using the equation $m(t) = a_0 + \sum a_i \sin[2\pi(f_i t + \phi_i)]$ ($i = 1, 2, 3$), where $m(t)$, a_0 , a_i , ϕ_i , and f_i are the calculated magnitude, zero point, semi-amplitude, phase, and frequency of the i th frequency. The dominant frequency of $f_1 = 34.119 \text{ c d}^{-1}$ (i.e., $P_{\text{puls}} \simeq 42.2$ min) with an amplitude of $4.82(\pm 0.44)$ mmag may be a reliable pulsating frequency. The value of Q for low-radial-order press mode (i.e., p -mode) oscillation of a δ -Scuti star is shorter than 0.04 d or less (Handler & Shobbrook 2002), which serves as a criterion to perform a rough mode identification. In order to further identify the pulsation mode, we estimated the phase shift and amplitude ratio between the B and V bands. For the frequency of f_1 from table 5, the observed phase shift is $+4.6$ for $B - V$, which

⁶ Period04 is available at (<http://www.univie.ac.at/tops/>).

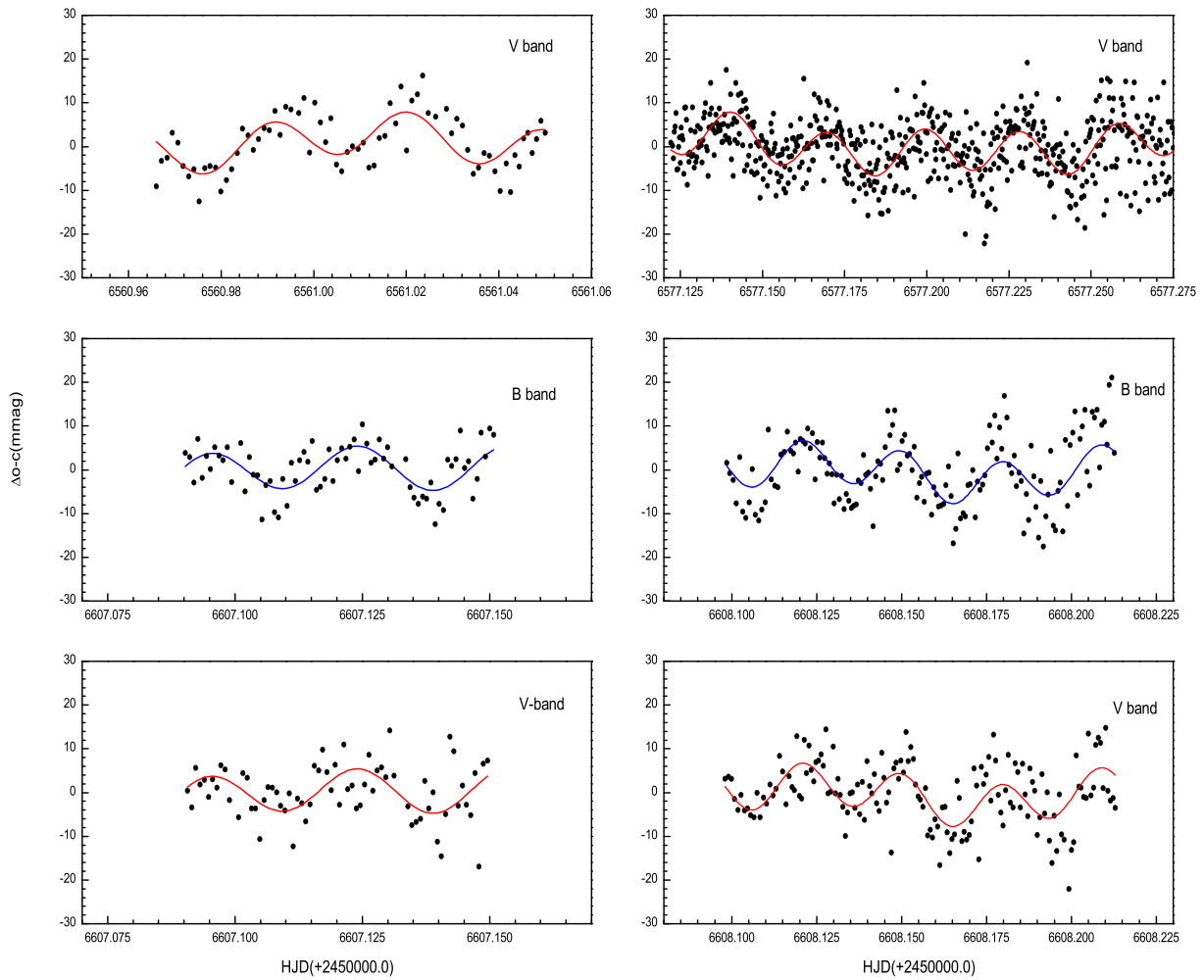


Fig. 5. Residual light curves with pulsations, observed by using the 85 cm telescope (top), and the 60 cm telescope (middle and bottom). The solid lines are plotted by three fitted frequencies from table 6. (Color online)

Table 6. Results of the multiple-frequency analysis.

Band	Frequency (c d^{-1})	Amplitude (mmag)	Phase (rad)	S/N	Q ($\times 10^{-2}$ d)
B	$f_1 = 34.125436(3)^*$	6.55 ± 0.67	0.9784 ± 0.1025	7.927	1.52
	$f_2 = 11.182094(9)$	1.74 ± 0.67	0.5956 ± 0.3860	4.152	4.63
V	$f_1 = 34.183144(3)$	4.47 ± 0.53	0.8968 ± 0.1176	13.365	1.52
	$f_2 = 6.455440(5)$	2.17 ± 0.53	0.9837 ± 0.2423	12.436	8.03
$B + V$	$f_3 = 12.904531(7)$	1.54 ± 0.53	0.4752 ± 0.3414	6.154	4.01
	$f_1 = 34.118590(1)$	4.82 ± 0.44	0.4875 ± 0.0918	9.264	1.52
$B + V$	$f_2 = 6.393003(3)$	1.97 ± 0.44	0.6553 ± 0.2246	8.378	8.11
	$f_3 = 13.645320(4)$	1.42 ± 0.44	0.1436 ± 0.3116	5.979	3.80

*The numbers in parentheses are the errors in the last decimal place.

means its radial pulsation according to the diagrams of Watson (1988) and Garrido, García-Lobo, and Rodríguez (1996). The amplitude ratio, B/V , of 1.47 may be a typical value compared with those for radial mode δ Scuti stars (Rodríguez et al. 1996). Therefore, the detected frequency of f_1 may be a p -mode pulsator.

Based on the eclipsing binaries with δ Scuti type primaries, Soydugan et al. (2006) and Soydugan and Kaçar (2013) successively derived two relations of $P_{\text{puls}} - P_{\text{orb}}$ (see figure 7a) and $\log P_{\text{plus}} - \log F$ (see figure 7b), where F is the gravitational pull exerted per gram of the matter on the surface of the primaries by the secondary companions.

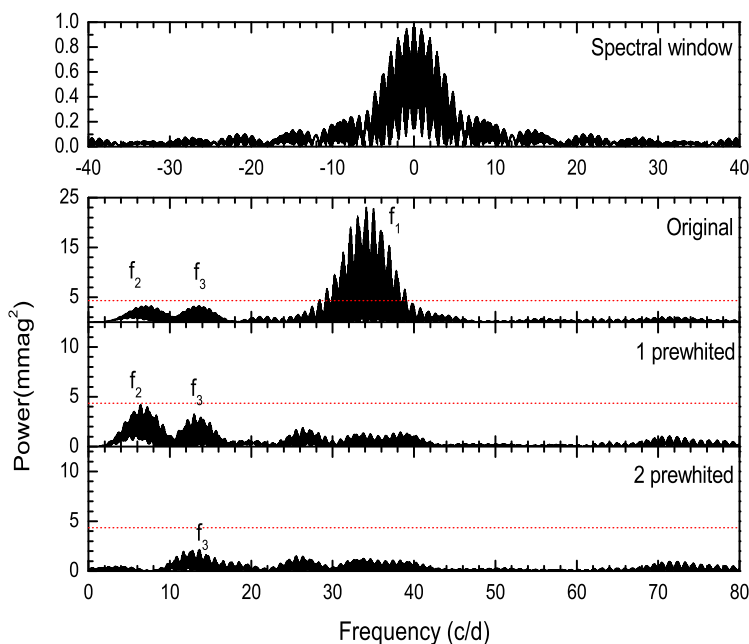


Fig. 6. Spectral window, power spectra, and significance limit (dotted line), which are derived from all the pulsating data in *B* and *V*. (Color online)

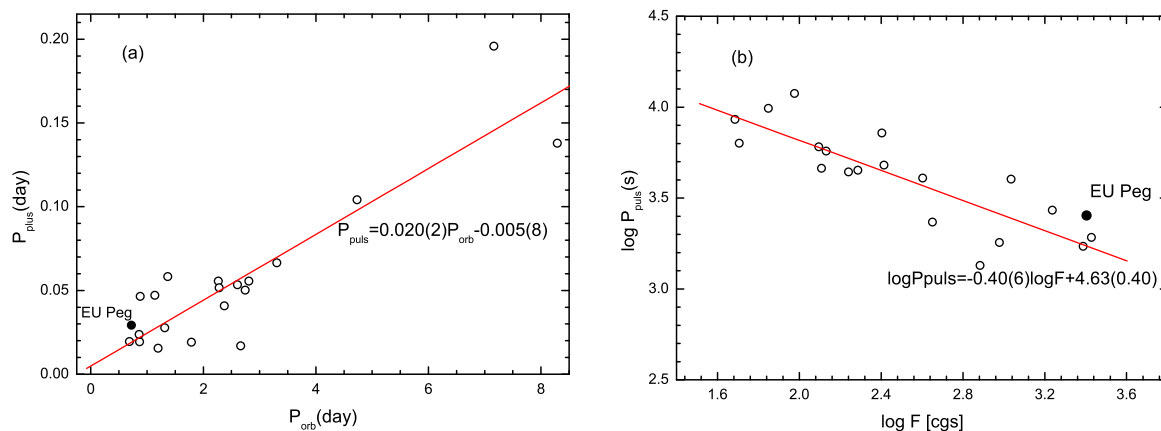


Fig. 7. (a) Relation between P_{orb} and P_{plus} taken from Soydugan et al. (2006), where the open circles represent 20 systems. (b) Relation between P_{orb} and P_{plus} taken from Soydugan and Kaçar (2013), in which the open circles refer to 19 binaries. The solid circle refers to the binary EU Peg in both panels. (Color online)

The primary pulsation of EU Peg (i.e., $P_{plus} = 0.029$ d) is also plotted as a solid circle in figure 7. From both panels, the observed main pulsation of EU Peg identifies the two relations (Soydugan et al. 2006; Soydugan & Kaçar 2013). For the short-period Algol-type binary EU Peg, the large gravitational force exerted from the secondary component, F , results in the short pulsating period. Figure 7 implies that when the orbital period decreases, the separation between the two components decreases. This will cause the gravitational force applied by the secondary companion onto the pulsating primary star to increase. Finally, the pulsating period will also decrease. According to the criterion given

by Breger et al. (1993), the two frequencies f_2 and f_3 are below the significance limit and may not be meaningful. This case occurs in the pulsating binary SX Dra (Soydugan & Kaçar 2013). Therefore, f_2 and f_3 with low amplitudes are needed for further identification in the future.

5 Discussions

From the previous analysis, EU Peg is a detached binary with a δ Scuti component, whose mass ratio is $q = 0.3105(\pm 0.0011)$. The fill-out factors for both components are $f_p = 86.7(\pm 0.6)\%$ and $f_s = 92.6(\pm 0.1)\%$,

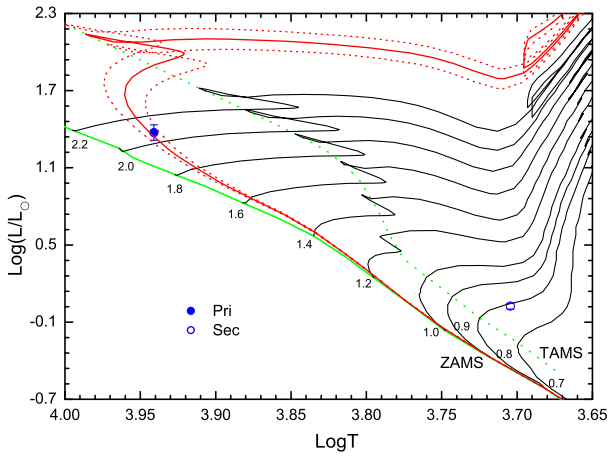


Fig. 8. Evolutionary locations of both components for the detached binary EU Peg. (Color online)

respectively. The light curves possess small pulsations; the dominant pulsating frequency of $f_1 = 34.12 \text{ c d}^{-1}$ is a p -mode pulsation. In order to obtain reliable frequency values, more data are needed in future observations. Due to the lack of spectroscopic elements (i.e., the semi-amplitudes of the radial velocity curves, K_1 and K_2), the absolute parameters are estimated by using Kepler's third law, $M_1 + M_2 = 0.134a^3/P^2$, in which $M_{1,2}$, a , and P are in units of M_\odot , R_\odot , and d, respectively.

Based on the assumed spectral type of A3V with a sub-type error, we adopted a mass of $M_1 = 2.60(\pm 0.30) M_\odot$ (Cox 2000). Using Kepler's third law and the photometric solution, we determined the other absolute parameters as listed in table 5. Both components are shown in figure 8; zero-age main sequence (ZAMS), terminal-age main sequence (TAMS), the evolutionary tracks, and isochrones for solar chemical compositions are taken from Girardi et al. (2000). The primary component between the ZAMS and TAMS lines is close to $\sim 2.0 M_\odot$ in an isochrone of ~ 0.47 Gyr, whose low luminosity and temperature with respect to its mass may result from the single-star evolutionary model. Meanwhile, the secondary component is near to the evolutionary track of $0.8 M_\odot$, and is far from the isochrone line. This may result from the binary interaction, which may represent its true evolutionary state.

From the period analysis, the $(O - C)$ curve possibly includes a cyclic variation. For close binaries, this kind of change may be attributed to either cyclic magnetic activity (Applegate 1992) or the light-time effect (Irwin 1952). For the early-type binary EU Peg, the less massive component may be an active star. The observed amplitude of the sinusoidal term in equation (2) may result from a change of the gravitational quadrupole moment, which can be computed by the equation from Lanza and Rodonò (2002)

as follows:

$$-9 \frac{R}{a} \frac{\Delta Q}{MR^2} = \frac{\Delta P}{P} \simeq \frac{2\pi A_{\text{mod}}}{P_{\text{mod}}}, \quad (3)$$

where a , R , and M are taken from table 5, and A and P_{mod} from equation (2). The value of $\Delta Q_2 = 6.71(\pm 1.24) \times 10^{-49} \text{ g cm}^2$ is much smaller than the typical order of 10^{-51} – 10^{-52} g cm^2 (Lanza & Rodonò 1999). Therefore, we could remove the magnetic activity, which may not work out in the secondary. On the other hand, another mechanism is the light-time effect due to the assumed third companion. From equation (2), we can easily obtain the value of $a_{12} \sin i' = A_{\text{mod}} \times c$, in which c and i' are the velocity of light and the orbital inclination. Then we can compute the mass function of the additional companion, $f(m)$, with the help of the following equation:

$$f(m) = \frac{4\pi^2}{GP_{\text{mod}}^2} \times (a_{12} \sin i')^3 = \frac{(M_3 \sin i')^3}{(M_1 + M_2 + M_3)^2}. \quad (4)$$

By the iteration method, we can determine the mass and radius for an orbital inclination i' . The minimum mass for the suggested third companion (i.e., $i' = 90^\circ$) is $M_3 = 0.23(\pm 0.04) M_\odot$ at a radius of $14.2(\pm 5.1) \text{ au}$. It may be a red dwarf with low luminosity (i.e., $\ell_3 \leq 1.0\%$), which is difficult to explore by spectroscopy.

In the non-conservative evolution for a close binary, the secular period changes should be the result of the net effect of mass transfer, mass loss, and angular momentum loss (Tout & Hall 1991). Due to the detached configuration for EU Peg, both components do not fill the Roche lobes, respectively. Assuming that the mass loss due to stellar wind is proportional to the total mass of system (i.e., $\dot{M} = \dot{M}_2 M/M_2$) and the escape radius is equal to the separation between both components (i.e., $R_{\text{es}} \simeq a$), we can obtain a simplified formula as follows (see Yang et al. 2013):

$$\frac{1}{P} \frac{dP}{dt} = \frac{5q^2 - q + 2}{q} \frac{\dot{M}}{M}, \quad (5)$$

where P , q , and M are the orbital period, mass ratio, and total mass, respectively. Inserting dP/dt and other parameters of the binary, we can determine a mass loss rate of $dM/dt = -4.96(\pm 0.72) \times 10^{-8} M_\odot \text{ yr}^{-1}$. Moreover, the possible additional companion in the EU Peg binary may extract angular momentum from the central system. Mass loss and angular loss result in the period decreasing. This will cause the orbit of the binary to shrink. Due to two components nearly filling their limiting Roche lobes, EU Peg finally may evolve from the detached configuration into the semi-detached one. More high-precision spectroscopy and

photometry for EU Peg are necessary to determine the absolute parameters more reliably, to explore the pulsating frequencies, and to search for any signature of the presence of a third component.

Acknowledgments

This research is partly supported by the Natural Science Foundation of China (grant nos. 11473009 and U1231102), and the Natural Science Research Project of Anhui Provincial Department of Education (grant no. KJ2017A850). Dr Yuangui Yang thanks Prof. Aigen Li for his invitation to collaborate on the study on planet-forming dust disks at the University of Missouri as a senior visiting scholar. The low-precision spectra were observed by the 2.4 m telescope at Lijiang station of YNAO and the 2.16 m telescope at XLs of NAOC. Many thanks are given to Professor Qing-Zhong Liu for providing the observing time for the 2.16 m telescope. The comprehensive photometry was carried out by the 60 cm and 85 cm telescopes at XLs of NAOC. We also made extensive use of the Simbad and NASA ADS databases.

Supplementary data

Supplementary data are available at [PASJ](https://academic.oup.com/pasj) online.

Complete listing of table 1.

References

- Aerts, C. 2007, in *IAU Symp. 240, Binary Stars as Critical Tools & Tests in Contemporary Astrophysics*, ed. W. I. Hartkopf et al. (Cambridge: Cambridge University Press), 432
- Agerer, F., Dahm, M., & Hübscher, J. 1999, *IBVS*, 4712, 1
- Agerer, F., & Hübscher, J. 2003, *IBVS*, 5484, 1
- Applegate, J. H. 1992, *ApJ*, 385, 621
- Breger, M., et al. 1993, *A&A*, 271, 482
- Budding, E., Erdem, A., Çiçek, C., Bulut, I., Soyduğan, F., Soyduğan, E., Bakiş, V., & Demircan, O. 2004, *A&A*, 417, 263
- Çakırlı, Ö., & İbanoglu, C. 2016, *New Astron.*, 45, 36
- Cox, A. N. ed. 2000, *Allen's Astrophysical Quantities*, 4th ed. (New York: Springer)
- Dal, H. A., & Sipahi, E. 2013, *PASA*, 30, e016
- Diethelm, R. 2000, *BBSAG Bull.*, 123, 1
- Diethelm, R. 2003, *IBVS*, 5438, 1
- Diethelm, R. 2011, *IBVS*, 5960, 1
- Diethelm, R. 2012, *IBVS*, 6011, 1
- Diethelm, R. 2013, *IBVS*, 6042, 1
- Dvorak, S. W. 2003, *IBVS*, 5378, 1
- Eggleton, P. P. 1983, *ApJ*, 268, 368
- Fan, Z., et al. 2016, *PASP*, 128, 115005
- Fan, Y.-F., Bai, J.-M., Zhang, J.-J., Wang, C.-J., Chang, L., Xin, Y.-X., & Zhang, R.-L. 2015, *Res. Astron. Astrophys.*, 15, 918
- Garrido, R., García-Lobo, E., & Rodríguez, E. 1990, *A&A*, 234, 262
- Girardi, L., Bressan, A., Bertelli, G., & Chiosi, C. 2000, *A&AS*, 141, 371
- Gough, D. 2000, in *ASP Conf. Ser.*, 203, *The Impact of Large-Scale Surveys on Pulsating Star Research*, ed. L. Szabados & D. Kurtz (San Francisco: ASP), 529
- Gray, R. O., & Corbally, C. J. 2009, *Stellar Spectral Classification* (Princeton: Princeton University Press)
- Handler, G., & Shobbrook, R. R. 2002, *MNRAS*, 333, 251
- Huber, D. 2015, in *Giants of Eclipse: The ζ Aurigae Stars and Other Binary Systems*, ed. T. B. Ake & E. Griffin (Heidelberg: Springer), 169
- Hübscher, J. 2005, *IBVS*, 5643, 1
- Hübscher, J. 2014, *IBVS*, 6118, 1
- Hübscher, J., & Agerer, F. 1996, *BAV Mitt.*, 93, 1
- Hübscher, J., Agerer, F., Frank, P., & Wunder, E. 1994, *BAV Mitt.*, 68, 1
- Hübscher, J., Agerer, F., & Wunder, E. 1992, *BAV Mitt.*, 60, 1
- Hübscher, J., Agerer, F., & Wunder, E. 1993, *BAV Mitt.*, 62, 1
- Hübscher, J., Agerer, F., & Wunder, E. 1995, *BAV Mitt.*, 79, 1
- Irwin, J. B. 1952, *ApJ*, 116, 211
- Juryšek, J., et al. 2017, *Open Eur. J. Variable Stars*, 179, 1
- Kaho, S. 1952, *Tokyo Astron. Bull.*, 30, 217
- Kim, S.-L., Lee, J. W., Lee, C.-U., Kang, Y. B., Koo, J.-R., & Mkrtichian, D. E. 2005, *IBVS*, 5598, 1
- Kreiner, J. M. 2004, *Acta Astron.*, 54, 207
- Kukarkin, B. V., et al. 1971, *General Catalogue of Variable Stars. Vol. III*, 3rd ed. (Moscow: Sternberg State Astronomical Institute of the Moscow State University)
- Lanza, A. F., & Rodonò, M. 1999, *A&A*, 349, 887
- Lanza, A. F., & Rodonò, M. 2002, *Astron. Nachr.*, 323, 424
- Lenz, P. 2004, *Commun. Asteroseismology*, 144, 41
- Lenz, P., & Breger, M. 2005, *Commun. Asteroseismology*, 146, 53
- Liakos, A., & Niarchos, P. 2015, in *ASP Conf. Ser.*, 496, *Living Together: Planets, Host Stars and Binaries*, ed. S.M. Rucinski et al. (San Francisco: ASP), 195
- Liakos, A., & Niarchos, P. 2017, *MNRAS*, 465, 1181
- Liakos, A., Niarchos, P., Soyduğan, E., & Zasche, P. 2012, *MNRAS*, 422, 1250
- Lucy, L. B. 1967, *Z. Astrophys.*, 65, 89
- Malkov, Y. O., Oblak, E., Snegireva, E. A., & Torra, J. 2006, *A&A*, 446, 785
- Mkrtichian, D. E., Rodríguez, E., Olson, E. C., Kusakin, A. V., Kim, S.-L., Lehmann, H., Gamarova, A. Y., & Kang, Y. W. 2005, in *ASP Conf. Ser.*, 333, *Tidal Evolution and Oscillations in Binary Stars: Third Granada Workshop on Stellar Structure*, ed. A. Claret et al. (San Francisco: ASP), 197
- Montgomery, M. H., & O'Donoghue, D. 1999, *Delta Scuti Star Newsletter*, 13, 28
- Nagai, K. 2008, *Var. Star Bull. Jpn.*, 46, 1
- Pamyatnykh, A. A., Dziembowski, W. A., Handler, G., & Piskunov, H. 1998, *A&A*, 331, 141
- Pickles, A., & Depagne, É. 2010, *PASP*, 122, 1437
- Rodríguez, E., Rolland, A., López de Coca, P., & Martín, S. 1996, *A&A*, 307, 539
- Ruciński, S. M. 1973, *Acta Astron.*, 23, 79
- Soyduğan, E., İbanoglu, C., Soyduğan, F., Akan, M. C., & Demircan, O. 2006, *MNRAS*, 366, 1289
- Soyduğan, E., & Kaçar, Y. 2013, *AJ*, 145, 87
- Tempesti, P. 1971, *IBVS*, 596, 1

- Tout, C. A., & Hall, D. S. 1991, MNRAS, 253, 9
Van Hamme, W., & Wilson, R. E. 2007, ApJ, 661, 1129
von Zeipel, H. 1924, MNRAS, 84, 655
Watson, R. D. 1988, Ap&SS, 140, 255
Wilson, R. E. 1979, ApJ, 234, 1054
Wilson, R. E., & Devinney, E. J. 1971, ApJ, 166, 605
Wilson, R. E., & Van Hamme, W. 2014, ApJ, 780, 151
Yang, Y.-G., Dai, H.-F., & Yin, X.-G. 2010, New Astron., 15, 392
Yang, Y.-G., Qian, S.-B., & Dai, H.-F. 2013, AJ, 145, 60
Yang, Y.-G., Wei, J.-Y., & Li, H.-L. 2014, AJ, 147, 35
Zejda, M. 2004, IBVS, 5583, 1
Zhang, X. B., Luo, C. Q., & Fu, J. N. 2013, ApJ, 777, 77
Zhou, A.-Y., Jiang, X.-J., Zhang, Y.-P., & Wei, J.-Y. 2009, Res. Astron. Astrophys., 9, 349